Colloidal and chemical stabilities of iron oxide nanoparticles in aqueous solutions: the interplay of structural, chemical and environmental drivers

Edwige Demangeat, Mathieu Pédrot, Aline Dia, Martine Bouhnik-Le Coz,
Fabien Grasset, Khalil Hanna, M. Kamagaté, Francisco Cabello-Hurtado

Environmental Science
Nano

Accepted Manuscript

Volume 3 | Number 1 | February 2016 | Pages 1–224

Environmental Science
Nano

rsc.li/es-nano

ISSN 2051-8153

ROYAL SOCIETY OF CHEMISTRY

PAPER
Joel A. Pedersen et al
Formation of supported lipid bilayers containing phase-segregated domains and their interaction with gold nanoparticles

175 YEARS

ROYAL SOCIETY OF CHEMISTRY

rsc.li/es-nano

Environmental significance statement

Amongst engineered nanoparticles, iron oxide nanoparticles (IONPs) appear particularly relevant toward the environment. Indeed, considering their potential uses in environmental fields (water and soil depollution, agrochemistry, etc.), it becomes critical to determine their behavior and fate in the environment. Their stability and reactivity are dependent upon the environmental parameters, and both intrinsic and surficial properties of IONPs. This work focused on the aggregation behavior of IONPs (especially magnetite, maghemite, hematite), their chemical transformation (oxidation of magnetite) and the impact of a surface coating that mimic natural interactions possibly occurring in the environment. Understanding these interactions and transformations will thus bring key insights regarding the mobility, bioavailability and chemical reactivity of IONPs in prevailing environmental conditions.

Environmental Science: Nano

ARTICLE

Colloidal and chemical stabilities of iron oxide nanoparticles in aqueous solutions: the interplay of structural, chemical and environmental drivers

E. Demangeat,[a] M. Pédrot,[a] A. Dia,[a] M. Bouhnik-le-Coz,[a] F. Grasset,[b] K. Hanna,[c] M. Kamagate[c] and F. Cabello-Hurtado[d]

Nanoparticle (NP) stability in aqueous environments is dependent upon many parameters including environmental conditions, NP concentrations as well as NP intrinsic characteristics. In this study, the effects of pH and surface modifications on the colloidal and chemical stabilities of nanosized magnetite (Fe_3O_4), maghemite (γ-Fe_2O_3) and hematite (α-Fe_2O_3) are investigated. Because changes in surface charge affect the size distribution of NP, pH plays a key role in driving the colloidal stability. More NP aggregation is observed at pH values close to the pH of zero point of charge (pHzpc). Coating of magnetite with humic acid (HA) and phosphatidylcholine (PC) affects the electrostatic interactions and then the colloidal behavior of NP. The rapid transformation of magnetite into maghemite through air oxidation results in significant modification of both surface charge and specific surface area of NP. Because the maghemite almost exclusively formed µm-scale aggregates, the colloidal stability of magnetite is expected to be hindered in oxic environments. For hematite, the particle size distribution data emphasize the influence of both pH and intrinsic surface properties in colloidal stability. These findings may have strong implications for an accurate prediction of the transformation and mobility of Fe-nanoparticles under environmentally relevant conditions and thus their fate in nature.

Introduction

Understanding the prevailing processes controlling chemical exchanges at soil/water interfaces is an environmental priority with regards to their impacts on both ecosystems and soil services, as well as water resources. Iron (Fe) oxides are ubiquitous minerals constituent of soils, sediments, aquifers and geological materials[1, 2]. Their origin is also anthropogenic as they are increasingly used in various fields such as for industrial, medical and environmental purposes[3-6]. Iron oxides nanoparticles (NP) respective stability, specific surface area, porosity, dissolution rate as well as transformation kinetics are controlled by their mineral structure and determine their fate and behaviour in the environment[7]. Amongst them, iron oxide nanoparticles, which also occur as ubiquitous phases in both soils and waters, play a critical role in the chemical dynamics resulting from environmental condition changes since nano minerals are highly reactive[8, 9]. In the natural conditions, only a small fraction of engineered iron oxide NP persists in its original form[10]. Biotransformation, oxidation/reduction, dissolution, precipitation, sorption and photochemical transformation may occur amongst other biogeochemical driven processes[11, 12]. In turn, this transformation can affect the aggregation, mobility,

biointeractions, uptake and fate of iron oxide NP in the environment as well as their impacts on the living environment[13].

Engineered iron oxide NP will become new tools for the treatment of contaminated waters and soils[14, 15]. As compared to conventional macroscale materials, nanomaterials exhibit a high surface-to-volume ratio and high reactivity. Thus, their colloidal size may give them high mobility in porous media and their properties allow them to be particularly suitable for the treatment of contaminated soils or aquifers. Iron oxide NP are involved in (i) the dechlorination of organic solvents (CCl_4, C_2Cl_4), (ii) the detoxification of pesticides (such as Lindane, DDT), (iii) the transformation of fertilizers (NO_3^-), and (iv) the immobilization of metals and metalloids (As, Pb, Cr, etc.)[16-18]. If remediation projects using iron oxide NP are currently focused on local-scale pollution, a scale change is initiated to act against diffuse pollution. Moreover, their use in nano-agrochemistry could be developed in the years ahead and would represent an intentional diffuse source of iron oxide NP within the environment[19]. A widespread use of iron oxide NP for *in situ* remediation or in agriculture also raises the question of their environmental compatibility.

Amongst engineered iron oxide NP of environmental concern, magnetite (Fe_3O_4), maghemite (γ-Fe_2O_3) and hematite (α-Fe_2O_3) are popular engineered iron oxide NP because of their biocompatibility and safety towards living organisms under certain conditions[20-22]. In particular, magnetite has shown an outstanding applicability in many research areas (e.g., semiconductor, magnetic resonance imaging, pigment, biomedicine, drug delivery, heterogeneous

a. *Univ. Rennes, CNRS, Géosciences Rennes - UMR 6118 – F- 35000 Rennes, France*
b. *Univ. Rennes, CNRS-Saint-Gobain-NIMS-UMI LINK 362-J-305-044, Tuskuba, Japan*
c. *Univ. Rennes, ENSCR- CNRS, ISCR (Institut des Sciences Chimiques de Rennes) - UMR 6226 F-35000 Rennes, France*
d. *Univ. Rennes, CNRS, Ecobio - UMR 6553 - F-35000 Rennes, France*

ARTICLE

[52] catalysis, and environmental remediation)[23, 24, 25] due to its unique magnetic properties and easy manipulation for control of morphologies, particle size, and Fe^{II}/Fe^{III} stoichiometry[26, 27]. However, determination of magnetite compositions which is highly sensitive to the preparation conditions is not a trivial task, particularly for nanoscale particles with a higher surface-to-volume ratio. Magnetite compositions range, without modification of the crystal structure, from that of stoichiometric Fe_3O_4, with 8 Fe^{3+} ions in tetrahedral and 8 Fe^{2+} + 8 Fe^{3+} ions in octahedral sites, to that of maghemite γ-$Fe^{III}_2O_3$ (considered as an extreme example of a non-stoichiometric magnetite) with only Fe^{3+} ions in both tetrahedral and octahedral sites. As compared to these iron oxides, hematite has only one type of cation, Fe^{3+} in its structure[28, 29].

In aqueous solution, iron oxides (IO) are amphoteric solids that acquire a surface charge in the protonation and deprotonation reactions of Fe-OH surface sites. The ensuing electrostatic, steric or combined stabilization layers that develop at the surface of the particles are significant in driving iron oxide NP colloidal stability[30]. The interfacial equilibrium at the surface of iron oxide NP is thus affected by the adsorption and desorption of the various constituents of the soil and soil solution in addition to the solution pH[31, 32]. The surface charge of iron oxide NP is also dependent upon their own structural organization such as isomorphic substitutions, which give iron oxide NP permanent charges.

As part of the Natural Organic Matter (NOM) occurring within soils and waters, macromolecular polyfunctional humic acid (HA), which displays a particular affinity for metal ions and their various acidic functional groups (carboxylic, phenolic, carbonyl), favours the formation of surface complexes on the Fe-OH sites of iron oxides via chemisorption[33]. As a consequence, interactions between iron oxide NP and HA should be further investigated. Several studies have shown that, in aqueous solution, the HA coating on iron oxide NP likely imparts a negative charge to the nanoparticle surfaces, increasing their surface potential and the ensuing propensity to stabilize iron oxide NP against aggregation[34-36]. Nevertheless, Hadju et al.[37] demonstrated that coating magnetite with HA could either foster or hinder Fe_3O_4-NP colloidal stability depending on the amount of HA present at the mineral surfaces. Other natural constituents such as amphiphilic phospholipids (integral major component of cell membranes) likely affect iron oxide NP stability. Using phospholipids as a coating on pyrite surfaces, Hao et al.[38] demonstrated that surface-bound lipids inhibit the iron core from oxidizing, even in the presence of bacteria, by forming a hydrophobic pocket[38, 39]. In addition, several authors have shown that a phospholipid coating likely decreases nanoparticle size dispersion and favours narrow-sized nanoparticles[40, 41]. Furthermore, the instability of magnetite in air causes NP to undergo a partial oxidation to maghemite (γ-Fe_2O_3), ending up with a core-shell structure in which the thickness of the oxidized layer is a function of the particle size[42, 43]. This phase transformation directly affects the surficial properties and internal characteristics of NP, which are deeply involved in driving iron oxide chemical stability and reactivity[44, 45].

In the environment, soils and soil solutions are prior interfaces for iron oxide NP interactions[46] occurring at mineral surfaces and in water. In addition to particle interactions, NP are prone to various chemical and physical modifications which foster the complexity of the reactions and likely affect both NP stability and reactivity. Electrostatic, steric or combined electrosteric forces can result from these interactions and promote repulsive forces whereas Van der Waals and magnetic dipolar interactions foster attraction between particles that likely aggregate. The intrinsic physicochemical properties of iron oxide NP (size, shape, surface area, chemistry, superparamagnetism, etc.), their ensuing high reactivity, together with the surrounding solution composition (dissolved species, pH, ionic strength, nanoparticle concentration), are the main drivers of iron oxide NP chemical and colloidal stability in aqueous media[47, 48].

Considering the geochemical, biological and technological significance of iron oxide NP[49], understanding the mechanisms of their stability may turn out to be relevant to unravel the fate and behaviour of iron oxide NP in the environment as well as their impacts on living organisms. Therefore, the aim of this work is to investigate the dual colloidal and chemical stability of magnetite NP in order to (i) understand the effects of their intrinsic properties (size, morphology, surface chemistry) and those of the environmental drivers (especially the effect of pH) on their aggregation state, (ii) assess the oxidation kinetics of magnetite, (iii) investigate the link between colloidal and chemical stability of NP, as well as (iv) identify the resulting environmental impacts. Hematite has also been studied to better understand the impact of intrinsic structural properties on iron oxide NP colloidal stability as the structure of hematite differs from both magnetite and maghemite. Indeed hematite NP size and morphology as well as internal crystal structure, generally confer a higher stability and crystallinity to hematite. Last, the method we chose to study the iron oxide NP aggregation state allowed us to study their size distribution over a wide range of sizes (that spread from one tenth of a nm to μm-scale aggregates) which allowed us to determine NP behavior in a context comparable to those observed in natural waters.

Experimental

Iron oxide nanoparticles and coated magnetite NP

Synthesis of bare iron oxide NP. Magnetite (Fe_3O_4) was prepared by the co-precipitation of iron salts according to the modified literature procedure[50, 51]. In brief, $FeCl_2.4H_2O$ (1.988 g) and $FeCl_3.6H_2O$ (5.406 g) were dissolved in 5 mL HCl (2 M) and 20 mL H_2O, respectively, and then mixed with magnetic stirring to obtain an iron solution with a molar ratio of Fe(II)/Fe(III) = 0.5. Magnetite NP were then precipitated by the dropwise addition of the iron salt solution into a 0.7 M NaOH-$NaNO_3$ base solution (250 mL). The black precipitate was left to settle in anaerobic conditions for a few hours to get rid of the supernatant. Three washings were then conducted in anaerobic conditions with deoxygenated deionized water and 5 10^{-3} M NaCl solution.

Maghemite (γ-Fe$_2$O$_3$) was synthesized following the method of Anna et al.[52], through the oxidation of the previously synthesized magnetite by adding 5 wt% NaOCl aqueous solution (16 mL) and sonicating for 2 hours. The solid product was magnetically separated and washed with water.

Hematite (α-Fe$_2$O$_3$) was synthesized by the forced hydrolysis of acid Fe(III) salt solutions at 98°C from 0.02 M Fe(NO$_3$)$_3$ following the protocol described in Schwertmann & Cornell (2003)[1].

Coatings with humic acid and phosphatidylcholines. Fe$_3$O$_4$-NP were coated with HA (Elliott Soil Humic Acid Standard IV) and PC (1, 2-bis (10, 12-tricosadiynoyl)-sn-glycero-3-phosphocholine - CAS Registry Number: 76078-28-9) to model a natural surface modification. The coating was carried out by physical interactions between the dissolved organic species (HA and PC) and a concentrated fraction of the Fe$_3$O$_4$-solution. Humic acid (0.2 g) was dissolved in 10 mL NaOH (1 M) and the obtained HA-solution was completed to 56 mL with deionized water. A similar PC-solution was obtained by dissolution in deionized water and ultrasonication. Fourty-four mL of a 6.0 g L^{-1} Fe$_3$O$_4$-NP solution was then added to each organic stock solution and each 100 mL of solution was shaken for 48 hours. At the end of the interaction, five washings were performed to remove the uncoated materials present in the supernatant after centrifugation.

Nanoparticle mass concentration measurement. The concentration of the iron oxide NP solution was inferred from the ICP-MS measurements of iron on triplicate samples for the iron oxide NP solutions and then recalculated regarding the total theoretical iron content of the minerals. Each NP sample was digested with sub-boiled nitric acid (14.6 M HNO$_3$) at 85°C, and then re-solubilized in 0.37 M HNO$_3$ after complete evaporation before measurement. Major- and trace-element concentrations were determined by ICP-MS (Agilent 7700x), using rhenium and rhodium as the internal standard. The international geostandard SLRS-5 was used to check the validity and reproducibility of the results[53].

Characterization

Size, morphology and surface properties. The morphology and individual particle size of Fe$_3$O$_4$, HA-Fe$_3$O$_4$, PC-Fe$_3$O$_4$, γ-Fe$_2$O$_3$ and α-Fe$_2$O$_3$ were determined using High Resolution Transmission Electron Microscopy (HR-TEM) with a JEOL2100F (voltage 200 kV). Specimens were prepared by drop-casting diluted Fe-NP suspensions on 300 mesh Au-grids supported with carbon film. The specific surface area of the iron oxides was determined by multipoint N$_2$–BET (Brunauer Emmett Teller) analysis using a Coulter (SA 3100) surface area analyzer.

The pH of zero point of charge was determined by potentiometric titrations, which were conducted with 1 and 2 g L^{-1} of solid at three ionic strengths (10^{-2}, 5.10^{-2}, and 10^{-1} M of NaCl). The suspension was purged with nitrogen gas to remove CO$_2$ in a double-walled Pyrex cell, which was kept at constant temperature by circulating water from thermostat. Titrations were conducted from 4 to 10 by addition of titrant solutions (HCl or NaOH).

Synthesized NP were characterized using X-ray powder diffraction (XRD). XRD data were collected with a Johanson monochromator using CuK$_\alpha$ radiation (λ = 1.5406 A). The X-ray diffractograms were found to be identical with the expected oxides.

Laser particle size analyses allowed the characterization of the size distribution of magnetite, maghemite, hematite and HA- and PC-

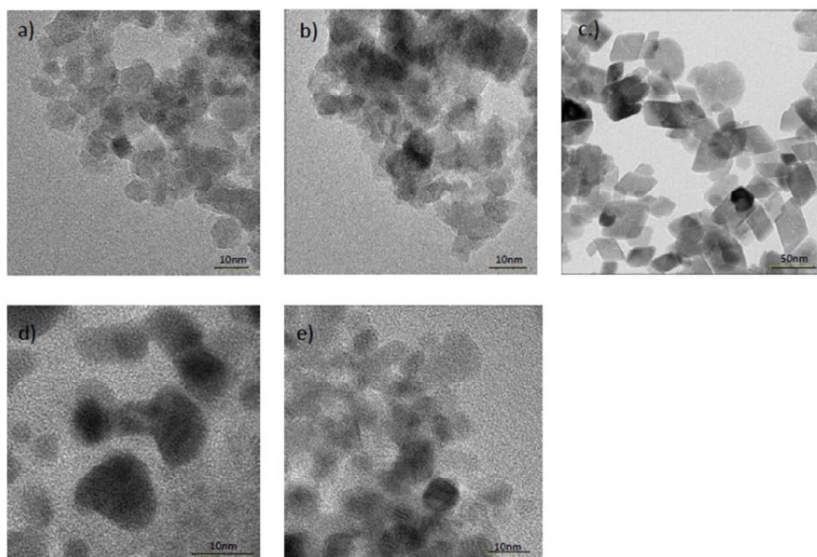**Fig. 1**: High Resolution TEM (HRTEM) images of a) Fe$_3$O$_4$, b) γ-Fe$_2$O$_3$, c) α-Fe2O3, d) HA-Fe$_3$O$_4$ and e) PC-Fe$_3$O$_4$

ARTICLE

Journal Name

263
264
265

NP	TEM (nm)	BET (m² g⁻¹)	pHzpc
Magnetite	7 ± 2	115	5.8
Maghemite	6 ± 2	131	7 - 8.4
Hematite	28 ± 5 39 ± 5	49	8.2

266
267
268
269
27 **Table 1**: Physicochemical properties of a) Fe_3O_4, b) γ-Fe_2O_3 and c) α-Fe_2O_3
27 obtained from TEM, BET analyses and potentiometric titration.
272

273 coated magnetite to study the colloidal stability and, conversely,
274 their aggregation behaviour. Assuming measurements on spherical
275 particles, the technique provided sizes amongst the 100 size classes
276 detected, which spread from 0.04 μm to 2500 μm. Analyses were
277 performed by the laser diffraction technique on a Cilas1180
278 analyzer. Measurements were taken on each bare iron oxide (Fe_3O_4,
279 γ-Fe_2O_3 and α-Fe_2O_3) and coated magnetite (HA-Fe_3O_4 and PC-
280 Fe_3O_4) at five different pH values (pH = 3, 4, 5, 6, 7.5). Particle size
281 measurements were performed by adjusting obscuration values
282 allowing for an optimal analysis. Then, the pH was equilibrated with
283 HCl and NaOH solutions (0.1 M and 0.1 M to 1.0 M, respectively)
284 until the target pH was reached.

285   **ATR-FTIR.** Attenuated total reflectance-Fourier transform
286 infrared (ATR-FTIR) spectra were recorded in the 780 - 1800 cm⁻¹
287 region on an IS50 Nicolet spectrometer equipped with a KBr beam
288 splitter and a liquid Nitrogen cooled MCT (Mercury Cadmium
289 Telluride) detector. A nine-reflection diamond ATR accessory
290 (Durasampl*IR* ™, SensIR Technologies) was used for acquiring
291 spectra of wet samples. The resolution of the single beam spectra
292 was 4 cm⁻¹. Prior to ATR-FTIR analyzes, tubes containing coated NP
293 were centrifuged at 4110 RCF for 30 min. Wet mineral pastes were
294 directly and uniformly applied to the diamond ATR crystal then
295 covered with a lid of a flow-through cell to prevent the evaporation
296 of water. ATR-FTIR spectra were then recorded immediately.

297 To monitor potential dissolution of NP, aliquots were collected at
298 each pH value, centrifuged and the supernatants were filtered using
299 5 KDa ultrafiltration cells (from Sartorius) in order to stop NP on the
300 filter. ICP-MS was then performed to measure total iron
301 concentration.

302   **Oxidation kinetics.** A NP suspension (2.5 g L⁻¹), prepared in
303 anoxic conditions, was placed outside the glove box under air
304 ambient environment to monitor the oxidation. The total
305 Fe(II)/Fe(III) ratio in suspension was then analyzed versus time over
306 nine days. For each sampling, two aliquots were placed in an
307 anaerobic chamber: the first aliquot contained bulk solution and
308 the second was filtered (0.2 μm, Whatman). NP suspension was
309 dissolved during 12h using 0.6 N HCl while filtered NP were directly
310 dissolved. Dissolved Fe(II) and Fe(III) concentrations were then
311 determined using the phenanthroline method[54, 55] and the bulk
312 Fe(II) content turned out to be very close to that determined by
313 acid digestion on the filtered solid. The amount of magnetite
314 bound-Fe(II) ([Fe(II)] bound = [Fe(II)]tot − [Fe(II)]aq) was used to
315 calculate the effective Fe(II)/Fe(III) ratio (denoted as (Fe(II)/Fe(III))
316 bound) in magnetite which was shown to vary with pH, as reported

317 in Cheng et al.[56]. [Fe(II)]tot is the total concentration of Fe(II) in the
318 suspension (solid + solution) and [Fe(II)]aq is the dissolved
319 concentration of Fe(II), measured after filtration (0.2 μm,
320 Whatman) of the magnetite suspension.
321

Results and discussion

Iron oxide NP physicochemical properties.

HR-TEM analyses provided images to assess the individual sizes and
325 shapes of the nanoparticles (Fig. 1). Magnetite and maghemite
326 oxides both displayed rounded shapes and similar sizes with
327 average diameters of 7 ± 2 nm and 6 ± 2 nm (Table 1), suggesting
328 that the oxidation of magnetite to maghemite did not impact the
329 particle size. Accordingly, BET surface area for maghemite (131 m²g⁻¹)
330 is relatively close to that of magnetite (115 m²g⁻¹) (Table 1).
331 Hematite displayed different morphologies with rhombohedral
332 shapes measuring 28 nm-wide and 39 nm-long on average, with a
333 surface area of 49 m²g⁻¹ (Table 1). No significant changes were
334 reported for neither HA- nor PC-coated magnetite from TEM
335 images, suggesting that the coating process did not modify the
336 morphology of magnetite. Although the surface area was not
337 determined for coated materials, no significant modification is
338 expected, according to previous findings[57].
339

ATR-FTIR spectroscopy

341 The IR spectrum recorded for of Fe_3O_4, HA-Fe_3O_4- and PC-Fe_3O_4
342 showed successful coating of HA and PC on magnetite surfaces (Fig.
343 2). In the spectra of HA-Fe_3O_4, the presence of an acid carboxylic
344 group was proven by the vibrational bands at 1410 cm⁻¹ and 1614
345 cm⁻¹ [58-60]. In the spectra of PC-Fe_3O_4, the absorption bands at 1239
346 cm⁻¹, 1088 cm⁻¹ and 970 cm⁻¹ were assigned to the presence of the
347 PO_4^{3-} group, suggesting that PC was coated on the magnetite
348 surface[61, 62].
349

Oxidation kinetics

351 The variation of total Fe(II)/Fe(III) ratio versus time for magnetite
352 suspension exposed to air is characterized by a two-steps' behavior.
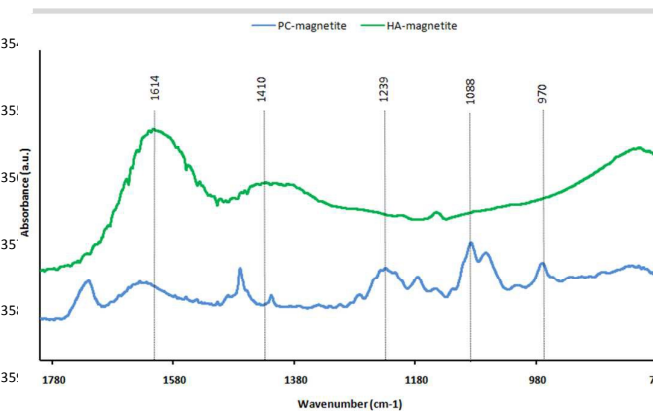353 Over the four first days (0-96 h), a sharp decrease in total

Fig 2: ATR-FTIR spectra of HA-magnetite and PC-magnetite in the range 780-1800 cm⁻¹ obtained from 0.5 g L⁻¹ NP suspensions at pH= 6.
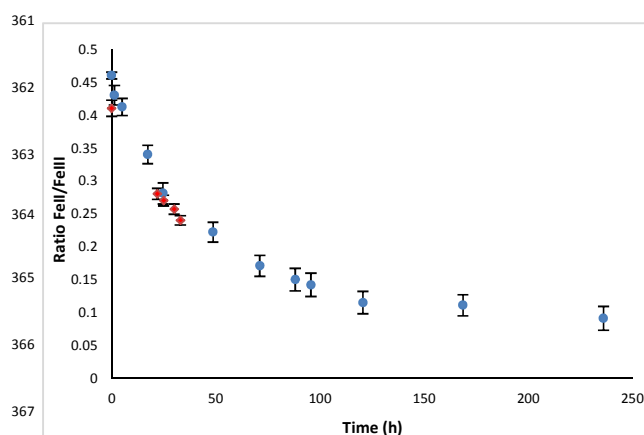
Fig 3: Evolution of the total Fe(II)/Fe(III) ratio (blue circles) and bound Fe(II)/Fe(III) ratio (red diamond) as a function of time. The reaction was performed with 2.5 g L^{-1} magnetite NP at pH = 7.5 in oxic conditions.

Fe(II)/Fe(III) ratio was observed (from 0.46 to 0.09). During this first stage, the bound Fe(II)/Fe(III) ratio was also decreased for magnetite as represented by red symbols in Figure 3. Then, the total Fe(II)/Fe(III) ratio slightly decreased beyond 5 days to reach 0.09 at the end of the experiment (236 h). As expected from the magnetite solubility at pH = 7.5[1], very little difference was observed between the total and bound Fe(II)/Fe(III) ratios.

Aggregation state

To assess the effect of pH and the effects of coating, laser diffraction analyses were performed on each iron oxide (Fe$_3$O$_4$, HA-Fe$_3$O$_4$, PC- Fe$_3$O$_4$, γ-Fe$_2$O$_3$ and α-Fe$_2$O$_3$) at five different pH values. For all experiments, the aggregation state was associated with the size distribution of the NP, which was described by considering the evolution of the sizes (based on number analyses) with the pH, occurrence rate and the polydispersity of the sizes (PDI, size range, mode and mean) of each iron oxide NP.

Effects of pH. The impact of pH on particle size distribution provides valuable information that could be used to distinguish the colloidal stability from the aggregation state of the various NP (Table 2). The different pH-dependent configurations highlighted the role of pHzpc in controlling NP aggregation through electrostatic interactions (Fig. 4). The effect of pH was studied by considering the evolution of the size distributions into four size classes (Fig. 4). The fractions were defined with regards to the most common sizes (representability) and depending on the way they vary with pH. However, it should be noted that fractions are not fully comparable to one another, as they were not spread out equally (i.e. fraction >0.4 μm (μm-scaled size class) as compared to 40-100 nm fraction (nm-scaled sizes)). The full-size distribution diagrams obtained from laser particle analyses as well as the precise occurrence rates (detectors) are provided in the Electronic Supporting Information (ESI).

It is worth noting that the total dissolved iron content was only detected in the magnetite suspension at pH = 3 and pH = 4 (90 and 23 μmol L^{-1} respectively). These values correspond to 1.4 % and 0.4 %, respectively, of the total iron amount in NP suspension. For HA- and PC-magnetite samples, no dissolved iron was detected regardless of the investigated pH.

Magnetite. The NP size distribution displayed two configurations: at pH = 5, 4 and 3, magnetite NP showed colloidal stability as compared to their size distribution at pH = 6 and 7.5. Magnetite size distribution at acidic pH was characterized by a high proportion of small NP (≤0.04 μm), and the occurrence of few dispersed μm-scaled aggregates (with sizes ranging between 1.6 μm and 32 μm). Such distribution allowed a large amount of NP not to sediment, as defined by Buffle et al.[63]. When the pH increased to 6 and 7.5, the number of coarser 100-400 nm and 40-100 nm-sized aggregates increased as the proportion of small aggregates decreased. This is consistent with the measured pHzpc = 5.8 (in accordance with previously published values[4]), since aggregation is commonly favoured at pH close to the pHzpc. Therefore, particles exhibiting negative charges likely formed coarser aggregates when the pH approached the pHzpc because of favorable electrostatic interactions[64].

	Magnetite		HA-Magnetite		PC-Magnetite			Maghemite			Hematite	
pH	6	5	4	3	7.5	5	4	7.5	6	5	7.5	5
Range (μm)	0.04 - 0.4; 1.6 - 32	0.04 - 0.4; 1.6 - 32	0.04 - 18	0.04 - 0.4; 1.1 - 19	0.04 - 0.4; 1.2 - 45	0.04 - 0.4; 1.1 - 40	0.04 - 0.4; 1.6 - 56	0.04 - 0.4; 1.6 - 28	0.04 - 0.4; 1.6 - 28	0.5 - 0.7; 1.1 - 28	0.04 - 6	0.04 - 0.4; 1.1 - 12
Mode (μm)	0.04	0.04	0.04	0.04	0.04	0.04	0.04	0.04	0.04	8	1.4	0.04
Mean (μm)	1.3	0.9	0.4	0.6	1.1	0.8	1.3	4.1	1.1	6.8	1.3	0.5
Median (μm)	0.07	0.04	0.04	0.07	0.07	0.04	0.07	0.2	0.04	7	1.2	0.04
PDI	1.38	2.74	13	5	1.9	3.4	1.3	0.56	2.06	0.72	4.8	7.6

Table 2: Size distribution characteristics of each NP at some typical pH (aggregation state versus colloidal stability). The table shows the size-range, mode, mean size, median value and the PDI (polydispersity index) of magnetite, HA-coated magnetite, PC-coated magnetite, maghemite and hematite. High PDI have values up to 1.0 and very high PDI are up to 2.0.
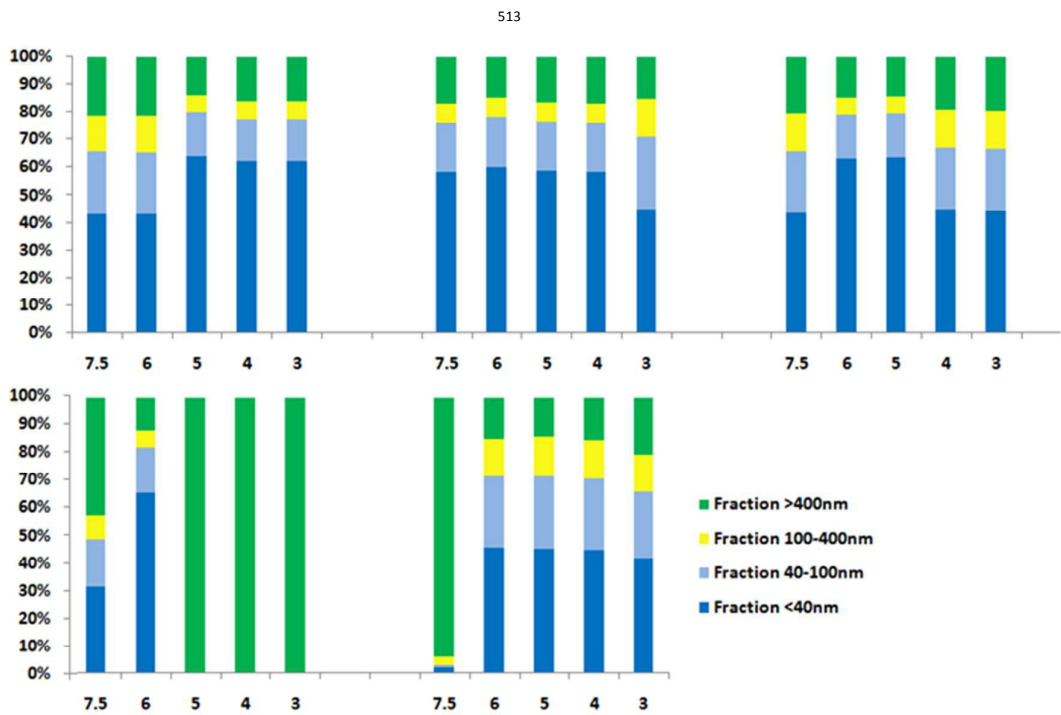
ARTICLE

Fig 4: Evolution of four typical size-class (proportion in %) with pH for a) magnetite, b) HA-magnetite, c) PC-magnetite, d) maghemite and e) hematite. Below the histograms, the table displayed the percentages of each fraction for typical pH (3, 4, 5, 6 and 7.5).

HA-Magnetite. HA-magnetite nanoparticles displayed both a continuous size distribution (pH = 4 to pH = 7.5) and a dual size distribution (pH = 3). In both cases, fraction below 0.04 μm was more important but their proportion decreased as the pH decreased from pH = 4 to 3. This decrease was accompanied by a slight increase in 40–100 nm-sized fraction and an increase in the proportion of coarser intermediate 100-400 nm NP size-class, which appeared to be more dependent upon pH than other fractions. The occurrence rate of the coarse aggregate fraction (>0.4 μm and >1.1 μm) remained constant regardless of the pH, hence a lower pH implied a moderated aggregation with small (≤0.04 μm) particles aggregating in only slightly coarser (0.05-0.4 μm) aggregates. Thus in HA-coated iron oxide NP, HA appeared to be an effective organic stabilizer towards iron oxide NP as previously demonstrated[65, 66].

PC-Magnetite. PC-magnetite nanoparticles highlighted two size distribution depending on the pH. At pH = 6 and 5, the size distribution was similar to that of bare magnetite at acidic pH (pH = 3 and pH = 4) where the colloidal stability displayed its maximum. At pH = 7.5, 4 and 3, Fe_3O_4-PC showed a similar size distribution to bare magnetite at pH >6, when it aggregated. When the pH decreased to pH = 4 and pH = 3, small aggregates (≤ 0.04 μm) were still the most common but in a lower proportion which was compensated by a higher amount of the three other coarser size fractions (in order: 40-100 nm; >1.6 μm and 100-400 nm). Although 100-400nm-sized aggregates were still the least common, this fraction was the most sensitive to pH as its proportion more than doubled from pH 6 and 5 to pH 4 and 3.

Maghemite. The size distribution displayed three configurations as distinct fractions whose proportions were strongly controlled by the pH. At a weak basic pH (pH = 7.5), the distribution was highly polydispersed and made up of coarse aggregates (>0.4 μm), which spread over a large size range. Maghemite NP displayed colloidal stability at pH = 6 with a size distribution similar to that of magnetite. However, when the pH decreased to a more acidic pH (pH = 5, 4 and 3), small-sized NP and NP aggregates disappeared to form much coarser aggregates with almost exclusively μm-scale sizes (>1 μm). Thus, the maghemite size distribution would be in good agreement with a high pHzpc close to 7.5[67, 68], as it became coarser than at pH = 6, but the high aggregation observed from pH = 3 to 5 suggested the possible implication of parameters other than electrostatic interactions to drive maghemite colloidal stability.

Hematite. The hematite size distribution showed two pH-dependent size distribution patterns. At pH = 7.5, the sizes were continuously distributed with a unique narrow size range composed of coarse homogeneous sizes displaying high polydispersity (multimodal distribution centered on 1.4 μm). When the pH decreased to pH = 6 and lower, the pH drastically modified the hematite size distribution to a more stable aggregation state[69] characterized by a monomodal distribution (0.04 μm) and higher abundance of finer particles (<0.4 μm). In accordance with the hematite pHzpc at pH = 8.2, hematite NP tended to aggregate when the pH reached pH = 7.5.

Effects of coating. The physico-chemical characteristics obtained from the combination of HR-TEM and ATR-FTIR showed

567 that HA have been successfully coated onto magnetite NP. 568 According to HR-TEM images, HA coating on magnetite did not 569 affect the original morphology and size of the precursor NP. As the 570 surface modification with HA provided primarily acidic functional 571 groups, the HA-coated magnetite pHzpc likely decreased to a lower 572 pH (pHzpc = 2.3). Accordingly, magnetite-HA promoted colloidal 573 stability from pH = 7.5 to pH = 4 because of repulsive electrostatic 574 interactions. The aggregation observed at pH = 3 - close to the new 575 pHzpc - would then be explained by the lack of negative surface 576 sites to compensate for the protonation induced by the H^+ 577 concentration increase in the aqueous solution. Both HA and bare 578 magnetite evidenced that the proportion of their size- fractions was 579 strongly controlled by the pH, which induced either colloidal 580 stability or aggregation. Nevertheless, HA coating promoted 581 smaller-sized aggregates as well as a narrower size distribution and 582 more homogeneous stable sizes (especially for coarser particles 583 (>0.4 μm)) compared to bare magnetite (Table 2). This enhanced 584 stabilization may stem from a HA steric barrier that helped maintain 585 a space between the particles to prevent the aggregation of NP[70, 71]. 586 Similar to the HA coating, the PC surface modification did not affect 587 the size and morphology of magnetite. Magnetite coated with PC 588 displayed a different colloidal behaviour as compared to bare 589 magnetite. As PC imparted both negative and positive surface 590 groups on the surfaces of the NP (glycerophosphate group, 591 trimethylethanolammonium group), and because of the complex 592 and heterogeneous surface structures that are generated by 593 adsorbed PC[72], PC-coated nanoparticles likely displayed variable 594 colloidal behaviours. As compared to magnetite, PC-NP showed 595 similar size proportions and repartition although the magnetite-PC 596 coarse fraction displayed a few large aggregates (hence its wider 597 size range, see Table 2) regardless of the pH. PC-NP were thus 598 probably able to form highly contrasted structures (according to 599 their size) suggesting that PC-coated magnetite did not entirely 600 depend on electrostatic interactions but also on steric forces[72].

601 **Effects of iron oxide intrinsic physicochemical properties.** The 602 oxidation of magnetite (Fe_3O_4) to maghemite (γ-Fe_2O_3) did not 603 change morphology and particle size. Maghemite still displayed a 604 higher surface area (131 m² g⁻¹) than magnetite (115 m² g⁻¹) and 605 oxidized NP very likely yielded intrinsic compositional differences. 606 These modifications probably resulted in a higher surface potential 607 thereby explaining the variable size distributions observed as the 608 pH changed. Maghemite NP aggregation was favoured at acidic pH 609 (equal or below 5), which would be in good agreement with their 610 high surface potential. Indeed, the tendency to form large 611 aggregates at these pH values likely resulted from a high energetic 612 barrier that had to be overcome at the mineral surfaces[73]. Indeed, 613 increasing NP surface to volume ratio leads to a higher surface 614 energy which induces aggregation between particles. As hematite 615 displayed a much lower surface area, the higher colloidal stability 616 observed over a wide pH range may result from a lower energetic 617 barrier at the surface of the particles in accordance with NP having 618 a relatively lower surface potential. Hematite stability would thus 619 be related, in part, to its smaller surface area and surface potential. 620 However, the typical aggregation behaviour of hematite NP

621 displaying coarse aggregates with homogeneous sizes suggests that 622 other mechanisms are involved at basic pH. Further investigations 623 are thus needed to fully assess iron oxide NP colloidal stability[74-76].

624 **Environmental perspectives.** Aggregation and stabilization have 625 significant effects on the mobility, reactivity and environmental fate 626 of NP. Once released in surface waters, unstable particles tend to 627 agglomerate, sediment or flocculate or they preferentially adsorb 628 onto bigger particles or surfaces[77]. As a result, aggregated NP that 629 form larger colloids with a possible smaller surface area are less 630 easy to transport and do not get through the soil as easily as smaller 631 particles[78]. As aggregated NP become less mobile, they may 632 become more ineffective in acting as nutrient carriers[79]. It is also 633 more difficult for these colloids to be taken up by plants and living 634 organisms as they are less soluble than their smaller counterparts[80]. 635 The dissolution of NP induces the mobilization of ions which are 636 likely complexed with molecules that foster their absorption by 637 plants and animals. In addition, depending on their concentration 638 and speciation as well as on the physiology of the organism that 639 absorbs it, metal atoms or ions can be either positive nutrients or 640 toxic elements. On the other hand, aggregation may directly affect 641 NP toxicity towards living organisms since smaller NP have been 642 shown to penetrate the cell walls of certain species more easily[81, 82]. 643 Considering the pH effect, the physicochemical properties of the 644 soil solution have to be considered in order to accurately assess the 645 fate of NP in the environment. NP intrinsic properties, such as their 646 surface chemistry, are also of prime importance since they are 647 involved in both electrostatic and steric interactions, which may 648 impact their dispersion, bioavailability and biocompatibility[83]. In 649 natural waters and surficial aerobic environments, NP likely 650 undergo many surficial modifications and become embedded in 651 matrixes or functionalized with specific molecules[84]. As a result, 652 these attached molecules can both passivate and/or confer their 653 own properties to mineral surfaces; e.g. polyanionic HA coating on 654 magnetite, resulting in a lower pHzpc and enhanced colloidal 655 stability. In addition, HA coating - as well as PC covering - might 656 passivate iron oxide NP surfaces to yield a steric barrier that 657 prevents Fe leakage from mineral surfaces and the ageing of the 658 magnetic core by oxidation. HA, which are ubiquitous in most 659 aquatic systems, display a specific affinity for iron oxide NP as well 660 as trace elements and therefore HA-iron oxide NP complexed 661 structures may also enhance ETM adsorption to NP. However, 662 although natural coatings demonstrated improved iron oxide NP 663 stability and reactivity, their effects depend upon the amount and 664 chemical composition of the substances[4].

665 The rapid oxidation of magnetite into maghemite is important since 666 iron plays an active redox catalytic role in many energy transfer and 667 electron transfer processes[85-87]. The iron oxide redox state also 668 plays a key role in specific anaerobic environments where Fe(II) and 669 Fe(III) are used as energetic catalysts for bacteria[88, 89]. Finally, the 670 transformation of magnetite into maghemite is also relevant 671 considering its adsorption capacity towards environmental 672 compounds[90]. Several questions are raised from these 673 environmental considerations, especially, what are the impacts of 674 these modifications regarding iron oxide NP reactivity?

Conclusions

The pH appears to be a key driver in controlling iron oxide NP colloidal behaviour as resulting from protonation and deprotonation reactions of surface hydroxyl-groups. Surface modifications also implied considerable effects on iron oxide NP colloidal stability as they promoted electrostatic interactions. In contrast to PC, HA was shown to be particularly efficient in enhancing magnetite colloidal stability. Magnetite seems to be highly unstable in aerobic conditions. The oxidation of magnetite into maghemite modified its surface chemistry and surface area, and these modifications resulted in higher aggregation at most pH values. Compared to maghemite, hematite appeared to be less sensitive to pH and displayed a lower surface area and surface potential. Both hematite and maghemite displayed high aggregation size distributions at different pH values.

Considering the widespread use of iron oxide NP and their subsequent release in the environment, their fate and behaviour in soils and natural waters raise many environmental questions not only in terms of their possible impacts on living organisms but also for their mobility and fate in ecosystems. Therefore, more attention should be paid for the understanding of colloidal and chemical stabilities of iron oxide NP as it is likely involved in many major interactions within the environment.

Acknowledgements

References

1   R. M. Cornell and U. Schwertmann, 2nd edition, http://trove.nla.gov.au/version/36973177, 2003, Edited by Wiley-VCH, 664p.

2   M. F. Hochella Jr, S. K. Lower, P. A. Maurice, R. L. Penn, N. Sahai, D. L. Sparks and B. S. Twining, *Science*, 2008, **139,** 1631.

3   A. Afkhami, M. Saber-Tehrani and H. Bagheri, *Desalination*, 2010, **263**, 240.

4   M. A. Ahmed, S. M. Ali, S. I. El-Dek and A. Galal, *Materials Science and Engineering B,* 2013,**178**, 744.

5   A. K. Gupta and M. Gupta, *Biomaterials,* 2005,**26**, 3995.

6   S. Laurent, J.-L.Bridot, L. Van der Elst and R. N. Muller, *Future Medicinal Chemistry,* 2010, **2(3)**, 427.

7   H. Guo and A. Barnard, *Journal of Materials Chemistry A*, 2013, **1**, 27.

8   M. Schindler and M. F. Hochella Jr., *Geology*, 2016, **44**, 515.

9   S. C. Löhr, D. T. Murphy, L. D. Nothdurft, R. Bohlar, S. Piazolo and C. Siegel, *Geochimica and Cosmochimica Acta*, 2017, **200**, 25.

10   C. W. Isaacson, M. Kleber and J. A. Field, *Environmental Science & Technology*, 2009, **43**,6463.

11   B. Nowack and T.D. Bucheli, *Environmental Pollution*, 2007, **150**, 5.

12   M. Auffan, J. Rose, J.-Y.Bottero, G. V. Lowry, J.-P.Jolivet and M.-R.Wiesner, *Nature Nanotechnology*, 2009, **4**, 634.

13   G. V. Lowry, K. B. Gregory, S. C. Apte and J. R. Lead, *Environmental Science & Technology*, 2012, **46**, 6893.

14   S. C. N. Tang, I. and M. C. Lo, *Water Research*, 2013, **47**, 2613.

15   M. Vitkova, S. Rakosova, Z. Michalkova, M. Komarek, *Journal of Environmental Management*, 2017, **186**, 268.

16   P. N. Dave and L. V. Chopda, *Journal of Nanotechnology*, 2014, **2014**, 1.

17   A. Aftabtalab, H. Sadabadi, CH. Shilpa Chakra, K. V. Rao, S. Shaker and E. Privilege Mahofa, *International Journal of Scientific & Engineering Research*, 2014, **5(1)**,1419.

18   S. R. Chowdhury and E. K. Yanful, *Journal of Environmental Management*, 2013, **129**, 642.

19   L. R. Khot, S. Sankaran, J. M. Maja, R. Ehsani and E. W. Schuster, *Crop Protection*, 2012, **35**, 64.

20   E. Navarro, A. Baun, R. Behra, N. B. Hartmann, J. Filser, A-J.Miao, A. Quigg, P. H. Santschi and L. Sigg, *Ecotoxicology*, 2008,**17**, 372.

21   A. Valdiglesias, N. Fernandez-Bertolez, G. Kiliç, C. Costa, S. Costa, S. Fraga, M. J. Bessa, E. Pasaro, J. P. Texeira and B. Laffon, *Journal of Trace Elements in Medicine and Biology*, 2016, **38**, 53.

22   R. Podila and J. M. Brown, *Journal of Biochemical and Molecular Toxicology*, 2013, **27(1)**, 50.

23   W. Wu, Z. Wu, T. Yu, C. Jiang and Woo-Sik Kim, *Sci. Technol. Adv. Mater*., 2015, **16**, 023501.

24   O. Veiseh, J. W. Gunn, M. Zhang, Advanced Drug Delivery Review, 2010, **62**, 304.

25   Y. Ju-Nam and J. R. Lead, *Science of the Total Environment*, 2008, **400**, 414.

26   A-H. Lu, E.L. Salabas and F. Schüt, Angew. Chem. Int. Ed., 2007, **46**, 1244.

27   D. Maity and D.C. Agrawal, *Journal of Magnetism and Magnetic Materials*, 2007, **308**, 46.

28   M. M. Can, M. Coskun and T. Firat, *Journal of Alloys and Compounds*, 2012, **542**, 241.

29   A. Lassoued, M. S. Lassoued, B. Dkhil, A. Gadri and S. Ammar, *Journal of Molecular Structure*, 2017, **1141**, 99

30   S. C. Pang, S. F. Chin and M. A. Anderson, *Journal of Colloid and Interface Science*, 2007, **311**, 94.

Journal Name
ARTICLE

31 L. Peng, P. Qin, M. Lei, Q. Zeng, H. Song, J. Yang, J. Shao, B. L. and J. Gu, *Journal of Hazardous Materials*, 2012,**209-210**,193.

32 E. Tombacz, Z. Libor, E. Illès, A. Majzik and E. Klumpp, *Organic Geochemistry*, 2004, **35**, 257.

33 A. M. Vindedahl, J. H. Strehlau, W. A. Arnold and R. L. Penn, *Environmental Science: Nano, Critical Review*, 2016, **3**, 1.

34 M. Baalousha, *The Science of the Total Environment*, 2009, **407**, 2093.

35 E. Illes and E. Tombacz, *Journal of Colloid and Interface Science,* 2006, **295**,115.

36 E. Tombacz, I.Y. Toth, D. Nesztor, E. Illés, A. Hadju, M. Szekeres and L. Vékas, *Colloids and Surfaces A: Physicochemical and Engineering Aspects*, 2013,**435**, 91.

37 A. Hajdú, E. Illés, E. Tombácz and I. Borbáth, *Colloids and surfaces A: Physicochemical and Engineering Aspects*, 2009, **347**, 104.

38 J. Hao, C. Cleveland, E. Lim, D. R. Strongin and M. A. A. Schoonen, *Geochemical Transactions*, 2006, **7:8**, 1.

39 X. V. Zhang, T. A. Kendall, J. Hao, D. R. Strongin, M. A. A. Schoonen and S. T. Martin, *Environmental Science & Technology*, 2006, **40**, 1511.

40 J. Giri, S. G. Thakurta, J. Bellare, A. K. Nigam and D. Bahadur, *Journal of Magnetism and Magnetic Materials*, 2005, **293**, 62.

41 S. Chatterjee, M. Krikorian, H. D. Gafney and B. Gersten, *Material Research Society*, 2011, **1061**, MM09-08.

42 R. Frison, G. Cernuto, A. Cervellino, O. Zaaharko, G. M. Colonna, A. Guagliardi and N. Masciocchi, *Chemistry of Materials*, 2013, **25**, 4820.

43 U. S. Khan, Amanullah, A. Manan, N. Khan, A. Mahmood and A. Rahim, *Material Science-Poland*, 2015, **33(2)**, 278.

44 I. Nedkov, T. Merodiiska, L. Slavov, R.E. Vandenberghe, Y. Kusano and J. Takada, *Journal of Magnetic Materials*, 2006, **300**, 358.

45 H. Shokrollahi, *Journal of Magnetism and Magnetic Materials*, 2017, **426**, 74.

46 L. Charlet G. Morin, J. Rose, Y. Wang, M. Auffan, A. Burnol and A. Fernandez-Martinez, *ComptesRendus Geoscience*, 2011, **343**, 123.

47 L. Chekli, S. Phuntsho, M. Roy, E. Lombi. E. Donner and H. K. Shon, *Water Research*, 2013, **47**, 4585.

48 W. Li, J. Wu, C. Kim and J. D. Fortner, *Environmental Science &Technology*, 2014, **48(20)**, 11892.

49 A. Navrotsky, L. Mazeina and J. Majzlan, *Science*, 2008, **319**, 1635.

50 R. Massart, *IEEE Transactions on Magnetics*, 1981, **17**,1247.

51 S. E. Khalafalla and G. W. Reimers, *IEEE Transactions on Magnetics*, 1980, **16(2)**, 178.

52 Z. B. Anna, B. Patricyja, J. Petr, E. Petrovsky, B. Pavel, H. Daniel, *Colloids and Surfaces B: Biointerfaces,* 2016, **141**, 389.

53 D. Yeghicheyan, C. Bossy, M. Bouhnik Le Coz, C. Douchet, G. Granier, A. Heimburger, F. Lacan, A. Lanzanova, T. C. C. Rousseau, J.L.   Seidel, M.   Tharaud, F.   Candaudap, J.

Chmeleff, C. Cloquet, S. Delpoux, M. Labatut, R. Losno, C. Pradoux Y. Sivry and J. E. Sonke, *Geostandards and Geoanalytical Research*, 2013, **37(4)**, 449.

54 C. A. Gorski and M. M. Sherer, *American Mineralogist*, 2010, **95**, 1017.

55 P. Komadel and J. W. Stucki, *Clays and Clay Minerals*, 1988, **36(4)**, 379.

56 W. Cheng, R. Marsac and K. Hanna, *Environ. Sci. Technol.*, 2018, **52 (2)**, 473.

57 J. Lohdia, G. Mandarano, N. J. Ferris, P. Eu and S. F. Cowell, *Biomedical Imaging and Intervention Journal*, 2010,**6(2)**, 1.

58 H. Niu, D. Zhang, S. Zhang, X. Zhang, Z. Meng and Y. Cai, *Journal of Hazardous Materials*, 2011, **190**, 559.

59 J.-F. Liu, Z.-S. Zhao and G.-B.Jiang, *Environmental Science & Technology*, 2008, **42**, 6949.

60 S. Koesnarpadi, S. J. Santosa, D. Siswanta and B. Rusdiarso, *Procedia Environmental Sciences* 30 (2015, 103.

61 S. Debnath, D. B. Hausner, D. R. Strongin and J. Kubicki, *Journal of Colloids and Interface Sciences*, 2010, **341**, 215.

62 Q.-C. Le, M.-H. Ropers, H. Terrisse and B. Humbert, *Colloids and Surfaces B: Biointerfaces*, 2014, **123**, 150.

63 J. Buffle, K. Wilkinson, S. Stoll, F. Montserrat, Z. Jingwu, *Environmental Science & Technology*, 1998, **32(19)**, 2899.

64 A. Kraynov and T. E. Müller, In *Applications of Ionic Liquids in Science and Technology*, 2011, Edited by Prof. S. Handy (516 pages), 235.

65 M. Pédrot, A.L. Boudec, M. Davranche, A. Dia, O. Henin, *Journal of Colloid and Interface Science*, 2011, **359**, 75.

66 D. Palomino and S. Stoll, *Journal of Nanoparticle Research*, 2013, **15(2)**, 1428.

67 N. Fauconnier, J. N. Pons, J. Roger and A. Bee, *Journal of Colloid and Interface Science*, 1997,**194**, 427.

68 L. Vayssieres, *J. Phys. Chem. C*, 2009, **113**, 4736.

69 K. Shimizu, S. V. Sokolov and R. G. Compton, *Colloid and Interface Science Communications*, 2016, **13**, 19.

70 S. Ghosh, W. Jiang, J. D. McClements and B. Xing, *Langmuir*, 2011*,* **27**, 8036.

71 S. F. Meideros, J. O.C. Filizzola, V. F.M. Fonseca, P. F.M. Oliveira, T. M. Silva, A. Elaissari and A. M. Santos, *Materials Letters*, 2015, **160**, 522.

72 R. Michel and M. Gradzielski, *International Journal of Molecular Science*s, 2012, **13**, 11610.

73 K. A. D. Guzman, M. P. Finnegan and J. F. Banfield, *Environmental Science & Technology*, 2006, **40**, 7688.

74 M. D. Carvalho, F. Henriques, L. P. Ferreira, M. Godinho and M. M. Cruz, *Journal of Solid State Chemistry*, 2013,**201**, 144.

75 E. Alp and N. Aydogan, *Colloids and Surfaces A: Physicochemical and Engineering Aspects*, 2016, **510**, 205.

76 D. Dickson, G. Liu, C. Li, G. Tachiev and Y. Kai, *The Science of the Total Environment*, 2012, **429**, 170.

77 A. M. Badawy, A. A. Hassan, K. G. Scheckel, M. T. Suidan and T. M. Tolymat, *Environmental Science and Technology*, 2013, **47**, 4039.

78 M. Komarek, A. Vanek and V. Ettler, *Environmental Pollution*, 2013, **172**, 9.

ARTICLE

79   C. Claudio, E. di Iorio, Q. Liu, Z. Jiang, V. Barron, *Journal of Nanoscience and Nanotechnology*, 2017, **17(7)**, 4449.

80   I. A. Mudunkotuwa and V. H. Grassian, *Journal of Environmental Monitoring*, 2011, **13(5)**, 1135.

81   J. Bauman, J. Köser, D. Arndt and J. Filser, *The Science of the Total Environment*, 2014, **484**, 176.

82   K. Powers, M. Palazuelos, B. M. Moudgil and S. M. Roberts, *Nanotoxicology*, *2007,* **1 (1)**, 42.

83   R. K. Das, S. K. Brar and M. Verma, *Trends in Biotechnology*, 2016, **34(6)**, 440.

84   D. Lin, S. D. Story, S. L. Walker, Q. Huang, W. Liang and P. Cai, *Environmental Pollution*, 2017, **228**, 35.

85   K. S. Siddiqi, A. ur Rahman, Tajuddin and A. Husen, *Nanoscale Research Letters*, 2016, **11**, 498.

86   H. Wu, J. J. Yin, W. G. Wamer, M. Zeng and Y. M. Lo, *Journal of Food and Drugs Analysis*, 2014, **22**, 86.

87   S. K. Chaudhuri, J. G. Lack, J. D. Coates, *Applied and Environmental Microbiology*, 2001, **67**, 2844.

88   M. Posfai, T. Kasama, E. T. Simpson, R. K. K. Chong and R. E. Dunin-Borkowski, *ActaCrystallica*, 2006**, 62**, 39.

89   J.-Y. Bottero, M. Auffan, J. Rose, C. Mouneyrac, C. Botta, J. Labille, A. Masion, A. Thill and C. Chaneac, *ComptesRendus Geoscience*, 2011, **343**, 168.

90   M. Davranche, A. Dia, M. Fakih, B. Nowack, G. Gruau, G. Ona-Nguema, P. Petitjean, S. Martin and R. Hochreutener, *Chemical Geology*, 2013,**335**, 24.